

Asymptotically flat vacuum initial data sets from a modified parabolic-hyperbolic formulation of the Einstein vacuum constraint equations

F. Beyer*, J. Frauendiener † and J. Ritchie‡

Department of Mathematics and Statistics, University of Otago, New Zealand.

April 8, 2020

Abstract

In this paper we continue earlier investigations [10, 12, 19] of evolutionary formulations of the Einstein vacuum constraint equations originally introduced by Rácz. Motivated by the strong evidence from these works that the resulting vacuum initial data sets are generically *not* asymptotically flat we analyse the asymptotics of the solutions of a modified formulation by a combination of analytical and numerical techniques. We conclude that the vacuum initial data sets generated with this new formulation are generically asymptotically flat.

1 Introduction

The Einstein vacuum constraint equations are a subset of the full Einstein field equations (EFE). The triple $(\Sigma, \gamma_{ab}, K_{ab})$ of a 3-dimensional differentiable manifold Σ , Riemannian metric γ_{ab} and a smooth symmetric tensor field K_{ab} on Σ is called a *vacuum initial data set* if it satisfies the *Einstein vacuum constraint equations*

$${}^{(3)}R - K_{ab}K^{ab} + K^2 = 0, \quad \nabla_a K^a_c - \nabla_c K = 0, \quad (1.1)$$

everywhere on Σ , where ∇_a is the covariant derivative associated with γ_{ab} , ${}^{(3)}R$ is the corresponding Ricci scalar and $K = K^a_a$ is the mean curvature. For this whole paper we agree that spatial abstract indices a, b, \dots are raised and lowered with the metric γ_{ab} .

Owing to the work of Choquet-Bruhat and Geroch [16, 23] we know that for every solution of the Einstein vacuum constraints there exists a unique maximal globally hyperbolic

*Email: fbeyer@maths.otago.ac.nz

†Email: joergf@maths.otago.ac.nz

‡Email: jritchie@maths.otago.ac.nz

development (a solution of the full vacuum EFE). Constructing solutions of the Einstein vacuum constraints is therefore the first crucial step in exploring solutions to the full vacuum EFE. The Einstein vacuum constraints Eq. (1.1) comprise a set of four nonlinear partial differential equations that constrain the twelve independent components of the two tensor fields γ_{ab} , K_{ab} . Solving Eq. (1.1) is therefore an under-determined problem, and to the best of our knowledge, there is no clear physically or geometrically preferred way to construct solutions.

One of the most successful methods for solving the constraints is the Lichnerowicz-York conformal approach (see [17] and references therein) which allows one to cast the constraints as a set of non-linear elliptic partial differential equations, which can in principle be solved as a boundary value problem. Solving the equations in this way can be challenging. However, there are several well established methods for doing this that have been very successful both from the analytical and the numerical perspective [4, 5]. Nevertheless, this approach is not without limitation. For example, mathematical problems have been known to arise when solutions with large mean curvatures are sought (see [2, 21] for an overview and references). Other more physical problems, such as spurious radiation [18, 25] also occur. Some researchers have therefore sought other methods of solving the constraints [13, 14, 26, 27].

In this work we focus on one such alternative approach, namely, the evolutionary formulations of the vacuum constraints introduced by Rácz in [30–32, 34]. In his work, Rácz introduced two ways to write the vacuum constraints: as a hyperbolic-algebraic system of PDEs on the one hand, and as a parabolic-hyperbolic system of PDEs on the other hand. In all these cases the constraints are solved as a Cauchy problem similar to earlier work in [3, 14]. First steps in investigating whether this approach has any advantages over more established methods have been carried out in [33] for the constraints of the Maxwell equations and in [22, 28] for the Einstein vacuum constraint equations. The main principal disadvantage of Rácz’s approach (in comparison to solving the vacuum constraints as an elliptic boundary value problem) is that it does not directly allow to control the asymptotics of the resulting vacuum initial data sets at spacelike infinity. This is problematic because certain physical quantities such as the total mass or the centre of mass (see for example [15, 36]), to name a few, are only well defined if the data sets satisfy particular asymptotic conditions. With no control over the asymptotics it is therefore possible that the method generates initial data sets that lack a physical interpretation. Exactly this issue has been explored recently in [10, 12, 19]. It was confirmed that generic solutions of these equations are not *asymptotically flat* (this notion is defined in Section 4 below). This is the case even for small (nonlinear) perturbations of asymptotically flat vacuum initial data sets. Other issues have been observed in [37].

In [12] we proposed an iterative approach to, at least partly, address the asymptotic flatness problem. In contrast to this, this paper here provides strong analytical and numerical evidence that a small change of how the free data for Rácz’s parabolic-hyperbolic formulation are specified is sufficient to guarantee asymptotic flatness of the vacuum initial data sets generated by this method. We note that a different, but similarly spirited modifi-

cation was suggested in [19]. As in [10, 12], we restrict most of our attention to Σ being the exterior region of an isolated gravitational source and we mostly assume that Σ is foliated by 2-spheres. This allows us to use the same numerical pseudo-spectral methods developed in [6, 8, 9, 11] based on the $\bar{\delta}$ - and the spin-weight formalism. We shall discuss that foliations based on topological 2-spheres imply the restriction that the constraint equations must be solved “towards spatial infinity” away from the sources of the gravitational field. We shall label this direction as the *increasing ρ -direction* where ρ is the *evolution parameter*. We remark that our focus here (as well as that of earlier works [10, 12]) on the *asymptotics* of these vacuum initial data sets will be overcome in future work. In this work here we are indeed not concerned with the properties of the solutions in the strong field regime, e.g. of apparent horizons. We also remark that the setup in [22], where foliations in terms of 2-planes are considered allowing for evolutions “towards the sources of the gravitation field”, is not well-suited to study the asymptotics because of the necessity of finite boundary conditions on the 2-planes.

The paper is outlined as follows: In Section 2 we briefly summarise the framework of 2 + 1-decompositions and introduce Kerr-Schild-like data sets. After a quick summary of Rácz’s *original* parabolic-hyperbolic formulation of the vacuum Einstein constraints in Section 3.1, we discuss our new modified version of these equations in Section 3.2. Section 4 is then devoted to the discussion of the asymptotics; we define the concept of *asymptotic flatness* and what it means for the 2 + 1-quantities introduced above. Now Section 5.1 yields analytical evidence for our claim that the vacuum initial data sets obtained with our modified parabolic-hyperbolic formulation are better behaved than those with the original formulation in as much as that generic solutions are asymptotically flat. We then support these analytical results by numerics in Section 6.

2 Preliminaries

2.1 The 2 + 1-decomposition of initial data sets

We now discuss Rácz’s original parabolic-hyperbolic formulation of the Einstein vacuum constraints. Further details can be found in [30–32, 34]. We use the same conventions as in [12].

Consider an arbitrary 3-dimensional manifold Σ , Riemannian metric γ_{ab} and smooth symmetric tensor field K_{ab} ; at this stage these are not required to satisfy any equation (such as the vacuum constraints). As before the Levi-Civita covariant derivative associated with γ_{ab} is labelled ∇_a . We suppose there exists a smooth function $\rho : \Sigma \rightarrow \mathbb{R}$ whose collection of level sets \mathcal{S}_ρ forms a foliation of Σ . This foliation yields a decomposition of $(\Sigma, \gamma_{ab}, K_{ab})$, in full analogy to standard 3 + 1-decompositions of spacetimes [1], as follows. The unit co-normal of any of the 2-surfaces \mathcal{S}_ρ is

$$N_a = A\nabla_a\rho, \tag{2.1}$$

where $A > 0$ is the *lapse*. The induced first and second fundamental forms are therefore,

respectively,

$$h_{ab} = \gamma_{ab} - N_a N_b, \quad (2.2)$$

$$k_{ab} = -\frac{1}{2} \mathcal{L}_N h_{ab}. \quad (2.3)$$

We shall label the covariant derivative associated with h_{ab} as D_a . The tensor field

$$h^a_b = \delta^a_b - N^a N_b$$

is the map that projects an arbitrary tensor defined at any point p in Σ orthogonally to a tensor that is tangent to S_ρ at p . If each index of a tensor field defined on Σ contracts to zero with N_a or N^a at all $p \in \Sigma$, then we call that it *intrinsic (to the foliation of surfaces S_ρ)*. Given an arbitrary tensor field on Σ we can create an intrinsic tensor field by contracting each index with h^a_b . In fact, any tensor can be uniquely decomposed into its intrinsic and its orthogonal parts, e.g.,

$$K_{ab} = \kappa N_a N_b + N_a p_b + N_b p_a + q_{ab}, \quad (2.4)$$

with

$$\kappa = N^a N^b K_{ab}, \quad p_a = h^c_a N^b K_{cb}, \quad q_{ab} = h^c_a h^d_b K_{cd}. \quad (2.5)$$

The field q_{ab} is symmetric and can be further decomposed into its trace and trace-free part (with respect to h_{ab}) as follows

$$q_{ab} = Q_{ab} + \frac{1}{2} q h_{ab}, \quad Q_{ab} h^{ab} = 0, \quad (2.6)$$

where the relations

$$q = h^{ab} q_{ab}, \quad Q_{ab} h^{ab} = 0 \quad (2.7)$$

hold and Q_{ab} is symmetric.

Now pick an arbitrary vector field ρ^a such that

$$\rho^a \nabla_a \rho = 1. \quad (2.8)$$

According to Eq. (2.1) there must exist a unique intrinsic vector field B^a , called the *shift*, such that

$$\rho^a = A N^a + B^a, \quad (2.9)$$

where A is the lapse in Eq. (2.1). Given ρ^a , we can write Eq. (2.3) as

$$k_{ab} = -A^{-1} \left(\frac{1}{2} \mathcal{L}_\rho h_{ab} - D_{(a} B_{b)} \right) =: A^{-1} k_{ab}^*. \quad (2.10)$$

We also define

$$\overset{\star}{k} := h^{ab} \overset{\star}{k}_{ab}. \quad (2.11)$$

Finally, the Ricci scalar ${}^{(3)}R$ associated with γ_{ab} can be written as

$${}^{(3)}R = {}^{(2)}R - \left(A^{-2} \overset{\star}{k}^2 + A^{-2} \overset{\star}{k}_{ab} \overset{\star}{k}^{ab} + 2A^{-1} D^a D_a A - 2 \left(A^{-1} \mathcal{L}_N \overset{\star}{k} - A^{-2} \mathcal{L}_N A \right) \right), \quad (2.12)$$

where the Ricci scalar associated with the induced metric h_{ab} is called ${}^{(2)}R$. The *intrinsic acceleration vector* is

$$v_b = N^a \nabla_a N_b = -A^{-1} D_b A. \quad (2.13)$$

2.2 Kerr-Schild-like data sets

In this subsection we introduce data sets (without imposing the constraints yet) of Kerr-Schild form. Such data sets were the basis of our previous work in [10, 12] and we shall continue to use them in particular in Section 6.1. In this paper now we introduce such data sets as follows.

Definition 1. A data set $(\Sigma, \gamma_{ab}, K_{ab})$ is called *Kerr-Schild-like* if $\Sigma = \mathbb{R}^3 \setminus \bar{B}$ where B is a ball in \mathbb{R}^3 and there exists a smooth function $V : \Sigma \rightarrow \mathbb{R}$ with $V < 1$, a smooth co-vector field l_a and a symmetric tensor field $\hat{\gamma}_{ab}$ such that

$$\gamma_{ab} = \delta_{ab} - V l_a l_b, \quad K_{ab} = \frac{\sqrt{1-V}}{2} (\nabla_a (V l_b) + \nabla_b (V l_a) - \hat{\gamma}_{ab}), \quad (2.14)$$

where δ_{ab} is the flat metric on Σ , $(\delta^{-1})^{ab}$ its inverse, and l_a satisfies the condition

$$(\delta^{-1})^{ab} l_a l_b = 1. \quad (2.15)$$

An example of a Kerr-Schild like data set is the standard ingoing Kerr-Schild Schwarzschild slice given by $l_a = \nabla_a r$, $V = -2m/r$ and $\hat{\gamma}_{ab} = 0$.

Let us now proceed by providing some useful formulas derived from this definition. For

$$\tilde{l}^a = (\delta^{-1})^{ab} l_b, \quad (2.16)$$

it follows

$$\tilde{l}^a l_a = (\delta^{-1})^{ab} l_a l_b = 1, \quad (2.17)$$

$$\gamma^{ab} = (\delta^{-1})^{ab} + \frac{V}{1-V} \tilde{l}^a \tilde{l}^b, \quad (2.18)$$

$$l^a = \frac{1}{1-V} \tilde{l}^a, \quad l^a l_a = \frac{1}{1-V}. \quad (2.19)$$

Suppose now we have chosen a smooth function ρ on Σ with the properties discussed in Section 2.1 giving rise to a foliation S in terms of level sets S_ρ diffeomorphic to the 2-sphere. We restrict to the case where l_a is normal to S_ρ , i.e.,

$$l_a = \pm f \nabla_a \rho, \quad (2.20)$$

with

$$f = \frac{1}{\sqrt{(\delta^{-1})^{ab} \nabla_a \rho \nabla_b \rho}}, \quad (2.21)$$

as a consequence of Eq. (2.15). From Eqs. (2.1), Eq. (2.20) and Eq. (2.19) we find that

$$N_a = \sqrt{1 - V} l_a, \quad (2.22)$$

which means that the lapse defined in Eq. (2.1) is

$$A = f \sqrt{1 - V}. \quad (2.23)$$

It now follows from Def. 1 and Eq. (2.2) that

$$h_{ab} = \delta_{ab} - l_a l_b. \quad (2.24)$$

Since

$$K_{ab} = \frac{2 - V}{4(1 - V)} (\nabla_a V N_b + \nabla_b V N_a) + \frac{V}{2} (\nabla_a N_b + \nabla_b N_a) - \frac{\sqrt{1 - V}}{2} \dot{\gamma}_{ab}, \quad (2.25)$$

Eq. (2.5) yields

$$\kappa = \frac{2 - V}{2(1 - V)^{3/2}} \tilde{l}^a \nabla_a V - \frac{\sqrt{1 - V}}{2} \dot{\gamma}_{ab} N^a N^b, \quad (2.26)$$

$$p_a = \frac{2 - V}{4(1 - V)} D_a V + \frac{V}{2} v_a - \frac{\sqrt{1 - V}}{2} \dot{\gamma}_{cb} h^c{}_a N^b, \quad (2.27)$$

$$q_{ab} = -V k_{ab} - \frac{\sqrt{1 - V}}{2} \dot{\gamma}_{cd} h^c{}_a h^d{}_b, \quad (2.28)$$

where v_a can be calculated from Eq. (2.13) and k_{ab} from Eq. (2.10) once a shift vector field B^a , and thereby the vector field $\rho^a = AN^a + B^a$, has been chosen. Notice that we can calculate B_a as

$$B_a = \rho^b h_{ab}. \quad (2.29)$$

The quantities q and Q_{ab} are given by Eq. (2.6) and $\overset{\star}{k}_{ab}$ and $\overset{\star}{k}$ are obtained from Eqs. (2.10) and (2.11).

3 Parabolic-hyperbolic formulations of the vacuum constraints

3.1 Rácz's parabolic-hyperbolic formulation of the vacuum constraints

Given the function ρ and the foliation in terms of 2-surfaces S_ρ generated by it as in Section 2.1, the vacuum constraints Eq. (1.1) can now be decomposed into their normal and intrinsic components, and, according to [32] yield the following system of equations:

$$\star k \mathcal{L}_\rho A + A^2 D^a D_a A - \star k B^a D_a A = \frac{1}{2} A^3 E + \frac{1}{2} A F, \quad (3.1)$$

$$\mathcal{L}_\rho q - B^a D_a q - A D_a p^a - 2 p^a D_a A = \star k^{ab} Q_{ab} + \frac{1}{2} q \star k - \star k \kappa, \quad (3.2)$$

$$\begin{aligned} \mathcal{L}_\rho p_c - B^a D_a p_c - \frac{1}{2} A D_c q - \kappa D_c A + Q^a{}_c D_a A + \frac{1}{2} q D_c A = p_a D_b B^a - A D_a Q^a{}_c \\ + \star k p_c + A D_c \kappa, \end{aligned} \quad (3.3)$$

where

$$E = {}^{(2)}R + 2\kappa q - 2p^a p_a - Q_{ab} Q^{ab} + \frac{1}{2} q^2, \quad (3.4)$$

$$F = 2(\partial_\rho \star k - B^a D_a \star k) - \star k_{ab} \star k^{ab} - \star k^2. \quad (3.5)$$

Observe that all quantities here are smooth *intrinsic* tensor fields. It is clear that while this means that all contractions with N^a or N_a vanish, contractions with ρ^a do not, e.g., $p_\rho := p_a \rho^a = p_a B^a$ as a consequence of Eq. (2.9). However such ‘‘components’’ p_ρ do clearly not constitute a further degree of freedom of the field p_a since $p_\rho = p_a B^a$ is fully determined by its ‘‘intrinsic components’’. Consistently with this, it is easy to check that the equation for p_ρ obtained by contracting Eq. (3.3) with ρ^c fully decouples from the remaining equations. We remark that instead of thinking of each field in the equations above as an intrinsic field on Σ , we could equivalently think of it as a 1-parameter family of fields on \mathbb{S}^2 defined by the pull-back along the ρ -dependent map $\Phi_\rho : \mathbb{S}^2 \rightarrow \Sigma$, $p \mapsto (\rho, p)$ to \mathbb{S}^2 . In the following we shall use abstract indices A, B, \dots for such ρ -dependent tensor fields on \mathbb{S}^2 . Indeed, all indices a, b, \dots in the equations above could be replaced by A, B, \dots , and, at the same type, each Lie-derivative along ρ^a by the derivative with respect to parameter ρ . All this is well-known for 3 + 1-decompositions of spacetimes and is therefore not discussed any further here.

Eqs. (3.1)–(3.3) suggest to group the various fields introduced above are as follows:

Free data The fields B_a , Q_{ab} , h_{ab} and κ are considered as freely specifiable everywhere on Σ . All of $\star k$, D_a , ${}^{(2)}R$, Q_{ab} and F (together with all of the index versions of these) as well as all coefficients in Eqs. (3.1)–(3.3) are fully determined by these on Σ .

Unknowns The quantities A , q and p_a are considered as the unknowns of Eqs. (3.1)–(3.3) once free data have been specified.

According to [31], it can be shown that given arbitrary smooth *Cauchy data*¹ for A , q and p_a on an arbitrary $\rho = \rho_0$ -leaf of the $2 + 1$ -decomposition of Σ , in addition to smooth *free data* everywhere Σ , the *Cauchy problem* of Eqs. (3.1)–(3.3) in the *increasing* ρ -direction is well-posed, i.e., the equations have a unique smooth solution A , q and p_a at least in a $\rho \geq \rho_0$ -neighbourhood of the initial leaf S_{ρ_0} , provided the *parabolicity condition* holds everywhere on Σ :

$$\overset{\star}{k} < 0. \tag{3.6}$$

Clearly, if $\overset{\star}{k}$ is positive instead, then the Cauchy problem is well-posed in the *decreasing* ρ -direction instead. In any case, Eqs. (3.1)–(3.3) is a quasilinear parabolic-hyperbolic system provided Eq. (3.6) holds everywhere.

It is important to remember that since the equation for the lapse is essentially a non-linear heat equation there is a significant difference between evolving in the “forward” and “backward” direction – a notion determined by the sign of $\overset{\star}{k}$ here. The Cauchy problem being well-posed in the forward direction (the increasing ρ -direction if $\overset{\star}{k} < 0$) means that the solutions are guaranteed to be smooth and well-behaved, while in the backward direction (the decreasing ρ -direction if $\overset{\star}{k} < 0$) they generically become “arbitrarily non-smooth after arbitrarily small evolution times”. Certain particular regular solutions may still be found in the backward direction, but the general lack of stability makes the backward problem unsuitable for numerical investigations. We therefore fully focus on the forward Cauchy problem here.

It is interesting to notice that $\overset{\star}{k}$ is fully determined by the free data. The condition Eq. (3.6) can therefore be verified *prior* to solving Eqs. (3.1)–(3.3). From Eqs. (2.3), (2.10) and (2.11) we deduce that $\overset{\star}{k}$ has the opposite sign than the mean curvature of the leaves of the foliation. Given Eq. (2.1) and the assumption that the lapse A is positive, it follows that *the Cauchy problem of Eqs. (3.1)–(3.3) is well-posed in the ρ -direction of the increasing area of the leaves of the foliation*. In the particular case that the foliation is of 2-sphere topology, as we shall restrict to for most of this paper, we shall align N^a with the outward-pointing direction. Since we expect this to be the direction of increasing area (at least asymptotically), we therefore anticipate Eq. (3.6) to hold and the increasing ρ -direction therefore to agree with the outward-pointing direction towards spatial infinity. In this setting all evolutions of Eqs. (3.1)–(3.3) must therefore be performed in the increasing ρ -direction.

3.2 Modified parabolic-hyperbolic formulation of the vacuum constraints

The system Eqs. (3.1)–(3.3) has been used in several works among which are [12, 19, 22, 28, 35]. The particular choice of how to split the fields into free data and unknowns is however not the only possibility. Motivated by previous studies [12, 19], which indicate an instability of these equations in the asymptotically flat setting, we now propose a small modification.

¹The Cauchy datum for A is assumed to be strictly positive everywhere without further notice.

The main result of our paper is that we can provide evidence that this instability observed for Eqs. (3.1)–(3.3) is resolved by this modification.

Recall that κ is one of the free data in the formulation introduced in Section 3.1 while q is one of the unknowns. Here now we propose to introduce a new free data field \mathcal{R} and then set

$$\kappa = \mathcal{R}q \quad (3.7)$$

where q continues to be an *unknown*. The equations resulting from this are obtained from Eqs. (3.1)–(3.3) by replacing all instances of κ with $\mathcal{R}q$:

$$\star k \mathcal{L}_\rho A + A^2 D^a D_a A - \star k B^a D_a A = \frac{1}{2} A^3 E + \frac{1}{2} A F, \quad (3.8)$$

$$\mathcal{L}_\rho q - B^a D_a q - A D_a p^a - 2p^a D_a A = \star k^{ab} Q_{ab} + \frac{1}{2} q \star k - \star k \mathcal{R} q, \quad (3.9)$$

$$\begin{aligned} \mathcal{L}_\rho p_c - B^a D_a p_c - A \left(\frac{1}{2} + \mathcal{R} \right) D_c q = p_a D_b B^a - A D_a Q^a{}_c + q \mathcal{R} D_c A - Q^a{}_c D_a A \\ + \star k p_c + A q D_c \mathcal{R} - \frac{1}{2} q D_c A, \end{aligned} \quad (3.10)$$

where, F takes the same form as before and E becomes

$$E = {}^{(2)}R - 2p^a p_a - Q_{ab} Q^{ab} + \left(2\mathcal{R} + \frac{1}{2} \right) q^2. \quad (3.11)$$

We shall refer to these equations as the *modified parabolic-hyperbolic system* while Eqs. (3.1)–(3.3) shall often be labeled as the *original parabolic-hyperbolic system*.

First we observe that this modification has changed the principal part of the system. It turns out that Eqs. (3.8)–(3.10) is still parabolic-hyperbolic. First, the principal part of Eq. (3.8) is unchanged (and is therefore parabolic provided the same parabolicity condition Eq. (3.6) as before holds), and, second, the subsystem Eqs. (3.9) – (3.10) is symmetrisable hyperbolic with symmetriser

$$\begin{pmatrix} \frac{1}{2} + \mathcal{R} & 0 \\ 0 & h^{ce} \end{pmatrix} \quad (3.12)$$

provided

$$\frac{1}{2} + \mathcal{R} > 0, \quad (3.13)$$

where h^{ce} is the intrinsic inverse of h_{ab} . We refer to Eq. (3.13) as the *hyperbolicity condition*. This now suggests the following choice:

Free data: The fields B_a , Q_{ab} , h_{ab} and \mathcal{R} are free data everywhere on Σ .

Unknowns: The fields A , q and p_a are the unknowns.

It follows that for arbitrary free data, for which both the parabolicity condition Eq. (3.6) and the hyperbolicity condition Eq. (3.13) hold, Eqs. (3.8)–(3.10) is a quasilinear parabolic-hyperbolic system and the *Cauchy problem* in the increasing ρ -direction is therefore well-posed (at least locally). Both conditions Eqs. (3.6) and (3.13) are conditions on the free data as before. We remark that our hyperbolicity condition here should not be confused with the hyperbolicity condition found by Rácz in his so-called algebraic-hyperbolic formulation [32].

It is not obvious why Eqs. (3.8)–(3.10) should be “any better” than Eqs. (3.1)–(3.3). The rest of the paper is about exactly this issue.

4 Asymptotics and radial expansions of data sets (without imposing the vacuum constraints yet)

As in [10, 12] we restrict now to the case $\Sigma = \mathbb{R}^3 \setminus \overline{B}$ where B is an arbitrary fixed ball in \mathbb{R}^3 in all of what follows. Moreover, we assume that the level sets of ρ are diffeomorphic to 2-spheres. This implies that we can assume that

$$\Sigma = (\rho_-, \infty) \times \mathbb{S}^2$$

for some $\rho_- > 0$ and we write the points in Σ as (ρ, p) with $\rho \in (\rho_-, \infty)$ and $p \in \mathbb{S}^2$. Observe carefully that we often use the same symbol ρ for the real parameter $\rho \in (\rho_-, \infty)$ and for the *function* ρ defined by $(\rho, p) \mapsto \rho$ used for the 2 + 1-decomposition. Consider now the manifold $\Sigma = (\rho_-, \infty) \times \mathbb{S}^2$ for some $\rho_- > 0$ as before. An initial data set (not necessarily a solution of the vacuum constraints²) is equivalently specified by a Riemannian metric γ_{ab} and smooth symmetric tensor field K_{ab} on Σ , or, by the fields $(A, \kappa, q, p_a, B_a, Q_{ab}, h_{ab})$ on Σ as in Section 2.1. We shall often speak of $(A, \kappa, q, p_a, B_a, Q_{ab}, h_{ab})$ as *the 2 + 1-fields associated with (γ_{ab}, K_{ab})* , or, equivalently of (γ_{ab}, K_{ab}) as *the initial data set associated with the 2 + 1 quantities $(A, \kappa, q, p_a, B_a, Q_{ab}, h_{ab})$* .

Let us now introduce some more notation and further structure. Given any $\rho \in (\rho_-, \infty)$, let $\Phi_\rho : \mathbb{S}^2 \rightarrow \Sigma$ be the map $p \mapsto (\rho, p)$ introduced earlier. Recalling the index conventions before, we let $(\Omega^{-1})^{AB}$ be the contravariant round unit metric on \mathbb{S}^2 . Sometimes it is useful to use standard polar coordinates (ϑ, φ) on \mathbb{S}^2 in terms of which the components of $(\Omega^{-1})^{AB}$ take the form of the matrix $\text{diag}(1, \sin^{-2} \vartheta)$. Given now an arbitrary smooth intrinsic tensor field $T_{a\dots b}$ on Σ , let $T_{A\dots B}$ be the (ρ -dependent) pull-back to \mathbb{S}^2 as discussed before. We then define the ρ -dependent norm

$$|T_{a\dots b}|^2 := T_{A'\dots B'} T_{A\dots B} (\Omega^{-1})^{AA'} \dots (\Omega^{-1})^{BB'}. \quad (4.1)$$

Notice that this is a norm only for *intrinsic* tensor fields on Σ . Given this we write $T_{a\dots b} = O\left(\frac{1}{\rho^k}\right)$ provided there is a uniform constant C such that $|T_{a\dots b}| \leq C\rho^{-k}$ sufficiently close

²Initial data sets that are *solutions* of the vacuum constraints are discussed in the sections following this one.

to $\rho = \infty$. We say that $T_{a\dots b}$ has an *asymptotic radial expansion of order k* (near $\rho = \infty$) provided

$$T_{a\dots b} = \sum_{i=0}^{k-1} T^{(i)}_{a\dots b} \rho^{-i} + O\left(\frac{1}{\rho^k}\right), \quad (4.2)$$

where the coefficients $T^{(i)}_{a\dots b}$ are smooth intrinsic tensor fields on Σ which do *not* depend on ρ , i.e., $\mathcal{L}_\rho T^{(i)}_{a\dots b} = 0$. If $T_{a\dots b} = O(1)$ then we say $T_{a\dots b}$ as an *asymptotic radial expansion of order 0*. In order to simplify the notation, we sometimes shall use these notions of the norm and the O -symbol for *general* tensor fields on Σ even when they are not intrinsic. In this case observe that this norm and this O -symbol are “completely blind” to all “transversal components” of the tensor field.

For the following it is also useful to define Ω_{ab} as the tensor field on Σ with the property $\rho^a \Omega_{ab} = 0$ whose pull-back along the map Φ_ρ above equals the covariant round unit metric on the 2-sphere for each ρ , i.e., the inverse of $(\Omega^{-1})^{AB}$. Notice carefully that Ω_{ab} defined this way is *not* intrinsic to the foliation (unless the shift vector field B^a vanishes). Its components with respect to adapted coordinates $(\rho, \vartheta, \varphi)$ on Σ as introduced before correspond to the matrix $\text{diag}(0, 1, \sin^2 \vartheta)$.

In all of what follows we shall assume without further notice that ρ_- is sufficiently large so that all 2 + 1-quantities are well-defined. Recall that asymptotically flat data sets have been studied by us before in [10, 12] where we have used the same definitions originally from [20].

Definition 2. *The triple $(\Sigma, \gamma_{ab}, K_{ab})$ with $\Sigma = \mathbb{R}^3 \setminus \overline{B}$ where B is a ball in \mathbb{R}^3 is called an asymptotically flat initial data set provided there exist coordinates $\{x^i\}$ on Σ such that the components of γ_{ab} and K_{ab} with respect to these coordinates satisfy, respectively,*

$$\gamma_{ij} = \left(1 + \frac{2M}{R}\right) \delta_{ij} + O\left(\frac{1}{R^2}\right), \quad K_{ij} = O\left(\frac{1}{R^2}\right), \quad (4.3)$$

in the limit

$$R = \left(\sum_{a=1}^3 (x^a)^2\right)^{1/2} \rightarrow \infty, \quad (4.4)$$

where $\delta_{ij} = \text{diag}(1, 1, 1)$. The quantity $M \in \mathbb{R}$ is called the ADM mass.

Asymptotic flatness therefore implies conditions on the asymptotics of 2 + 1 quantities associated with an initial data set $(\Sigma, \gamma_{ab}, K_{ab})$; see also [10, 12, 19].

Result 1 (Asymptotically flat data sets). *A data set $(\Sigma, \gamma_{ab}, K_{ab})$ is asymptotically flat with ADM mass M provided all corresponding 2 + 1-fields have the following asymptotic radial expansions:*

1. *The expansion of A is of order 2 with $A^{(0)} = 1$ and $A^{(1)} = M = \text{const}$.*

2. The expansion of B_a is of order 1 with $B_a^{(0)} = 0$.
3. The expansion of h_{ab} is of the form $\rho^{-2}h_{ab} = \Omega_{ab} + O(\rho^{-2})$.
4. The expansion of q is of order 2 with $q^{(0)} = q^{(1)} = 0$.
5. The expansion of p_a is of order 1 with $p_a^{(0)} = 0$.
6. The expansion of Q_{ab} is $Q_{ab} = O(1)$.
7. The expansion of κ is of order 2 with $\kappa^{(0)} = \kappa^{(1)} = 0$.

Proof. As before we assume that $\Sigma = (\rho_-, \infty) \times \mathbb{S}^2$ with radial parameter ρ . For the following it is useful to introduce coordinates $(\rho, \vartheta, \varphi)$ on Σ where (ϑ, φ) are standard polar coordinates on each leaf diffeomorphic to \mathbb{S}^2 . As mentioned before the components of Ω_{ab} with respect to these coordinates take the form $\text{diag}(0, 1, \sin^2 \vartheta)$. Under the assumptions above, the components of γ_{ab} with respect to these coordinates are

$$\gamma_{\alpha\beta} = \text{diag} \left(1 + \frac{2A^{(1)}}{\rho}, \rho^2, \rho^2 \sin^2 \vartheta \right) + \begin{pmatrix} O\left(\frac{1}{\rho^2}\right) & O\left(\frac{1}{\rho}\right) & O\left(\frac{1}{\rho}\right) \\ O\left(\frac{1}{\rho}\right) & O(1) & O(1) \\ O\left(\frac{1}{\rho}\right) & O(1) & O(1) \end{pmatrix},$$

where the O -symbol for each component here is interpreted as that for *scalar functions* on \mathbb{R}^3 . With respect to the new radial coordinate

$$R = \rho - A^{(1)},$$

the components of γ_{ab} are therefore

$$\gamma_{\alpha'\beta'} = \omega^2 \text{diag} (1, R^2, R^2 \sin^2 \vartheta) + \begin{pmatrix} O\left(\frac{1}{R^2}\right) & O\left(\frac{1}{R}\right) & O\left(\frac{1}{R}\right) \\ O\left(\frac{1}{R}\right) & O(1) & O(1) \\ O\left(\frac{1}{R}\right) & O(1) & O(1) \end{pmatrix},$$

where $\omega^2 = 1 + \frac{2A^{(1)}}{R}$. Transforming the polar coordinates (R, ϑ, φ) to Cartesian coordinates in the standard way, we finally obtain

$$\gamma_{ij} = \omega^2 \text{diag} (1, 1, 1) + \begin{pmatrix} O\left(\frac{1}{R^2}\right) & O\left(\frac{1}{R^2}\right) & O\left(\frac{1}{R^2}\right) \\ O\left(\frac{1}{R^2}\right) & O\left(\frac{1}{R^2}\right) & O\left(\frac{1}{R^2}\right) \\ O\left(\frac{1}{R^2}\right) & O\left(\frac{1}{R^2}\right) & O\left(\frac{1}{R^2}\right) \end{pmatrix},$$

as required for asymptotic flatness. We can therefore identify $A^{(1)}$ with the quantity M . The same arguments applied to K_{ab} yield that the condition for asymptotic flatness is satisfied provided $\kappa^{(0)} = \kappa^{(1)} = 0$, $p_a^{(0)} = 0$ and $q_{ab} = O(1)$ (which is equivalent to assumptions 4 and 6). \square

Given an arbitrary initial data set (not necessarily solving the constraints), then we can show that³ $\overset{\star}{k} = -2/\rho + O(1)$, and therefore $\overset{\star}{k} < 0$ for sufficiently large ρ ; cf. Eq. (3.6). Since general asymptotically flat data sets of the form in Result 1 imply that $\mathcal{R} = O(1)$, they can only be used as *backgrounds* for solving the modified system Eqs. (3.8)–(3.10), if we impose additional conditions to ensure Eq. (3.13). We discuss this issue below.

Here now we return briefly to Kerr-Schild-like data sets introduced in Section 2.2. To this end we introduce an arbitrary smooth function r on Σ with the property that

$$r = \rho + O(\rho^{-1}); \quad (4.5)$$

notice carefully that we demand that no $O(1)$ -term is present in this expansion. In terms of this function r , we assume that the flat metric δ_{ab} in Def. 1 takes the form

$$\delta_{ab} = \nabla_a r \nabla_b r + r^2 \Omega_{ab} \quad (4.6)$$

where Ω_{ab} was introduced above. Given this it is straightforward to show that the function f in Eqs. (2.20) and (2.21) is $f = 1 + O(\rho^{-2})$, that $\rho^{-2} h_{ab} = \Omega_{ab} + O(\rho^{-2})$ as a consequence of Eq. (2.24) and that $B_a = O(\rho^{-1})$ from Eq. (2.29). It follows from Result 1 and the formulas in Section 2.2 that the Kerr-Schild-like data set is asymptotically flat provided V has an asymptotic radial expansion of order 2 where $V^{(0)} = 0$ and $V^{(1)} = \text{const}$. In this case the ADM mass is $M = -V^{(1)}/2$.

5 Vacuum initial data sets obtained by the modified parabolic-hyperbolic system

5.1 The spherically symmetric case

In this section we analyse the asymptotics of vacuum initial sets obtained as solutions of Eqs. (3.8)–(3.10). Recall that Eqs. (3.1)–(3.3) have been analysed in [12, 19]. We present evidence that all the instabilities regarding asymptotic flatness, which were found for the original system, are resolved by this modification.

The general idea here and in the following is to pick a *background* initial data set (in general not a solution of the constraints) which is asymptotically flat according to Result 1 in a first step. From this background data set, we then read off the free data for solving Eqs. (3.8)–(3.10) in a second step. We start this subsection with the simpler spherically symmetric case in which Eqs. (3.8)–(3.10) reduces to a system of ordinary differential equations. To this end we consider backgrounds in Kerr-Schild-like form as in Section 2.2 with Eqs. (4.5) – (4.6). We impose spherical symmetry by requiring that V only depends on ρ and that $r = \rho$. We also choose $\dot{\gamma}_{ab} = 0$. The 2 + 1-quantities defined by this are

$$Q_{ab} = 0, \quad h_{ab} = \rho^2 \Omega_{ab}, \quad B_a = 0, \quad \mathcal{R} = \frac{(2 - V)\rho}{4(1 - V)} \frac{\partial_\rho V}{V}, \quad (5.1)$$

³Without going into technical details we assume here that the O -symbol does not only control the fields themselves as discussed before, but also sufficiently many of their derivatives in the natural way.

and

$$q = \frac{2V}{\rho\sqrt{1-V}}, \quad p_a = 0, \quad A = \sqrt{1-V}. \quad (5.2)$$

In order to ensure that \mathcal{R} is a smooth quantity, we assume that $\partial_\rho V/V$ is well-defined and finite for all $\rho > 0$.

We use Eq. (5.1) now as a background to determine the free data for the modified parabolic-hyperbolic system Eqs. (3.8)–(3.10). Since q , p_a and A are supposed to be found as solutions of the equations we therefore ignore Eq. (5.2). In order to appeal to spherical symmetry, we look for solutions under the restriction $p_a = 0$ and where the unknowns A and q only depend on ρ . With this, Eqs. (3.8)–(3.10) take the form

$$\partial_\rho q = -\frac{2}{\rho} \left(\frac{1}{2} - \mathcal{R} \right) q, \quad (5.3)$$

$$\partial_\rho A = -\frac{\rho}{4} \left(\frac{2}{\rho^2} + \left(2\mathcal{R} + \frac{1}{2} \right) q^2 \right) A^3 + \frac{1}{2\rho} A. \quad (5.4)$$

It is surprising⁴ that for any function V which satisfies the previous restrictions, we can write down the general solution explicitly as

$$q = \frac{2\mathcal{C}V}{\rho\sqrt{1-V}}, \quad (5.5)$$

$$A = \sqrt{\frac{(1-V)\rho}{\rho - 2m - (\rho - 2m)V + \rho\mathcal{C}^2V^2}}, \quad (5.6)$$

where $m, \mathcal{C} \in \mathbb{R}$ are free constants. It is interesting to notice that this only agrees with Eq. (5.2) if $\mathcal{C} = 1$ and $V = -2m/\rho$. Irrespective of the choice of V , the Hawking mass [24] of each surface S_ρ of the resulting vacuum initial data set turns out to be

$$m_H = m, \quad (5.7)$$

and is therefore independent of ρ .

Since we study vacuum solutions in somewhat more detail in the next subsection, let us now consider the following specific choice of the function V

$$V = -\frac{\mathcal{V}}{\rho}, \quad (5.8)$$

for an arbitrary constant $\mathcal{V} \in \mathbb{R}$. From the discussion at the end of Section 4, the background data set above is therefore asymptotically flat with mass $\mathcal{V}/2$. With this choice the solutions Eq. (5.5)–(5.6) have the following asymptotic expansions

$$A = 1 + \frac{m}{\rho} + O\left(\frac{1}{\rho^2}\right), \quad q = -\frac{2\mathcal{C}\mathcal{V}}{\rho^2} + O\left(\frac{1}{\rho^3}\right), \quad \kappa = \mathcal{R}q = \frac{\mathcal{C}\mathcal{V}}{\rho^2} + O\left(\frac{1}{\rho^3}\right). \quad (5.9)$$

⁴This is not possible for the original system; see [12].

It is a consequence of Result 1 that the resulting vacuum initial data set is therefore *asymptotically flat with ADM mass* $m \in \mathbb{R}$ *irrespective of the choice of* $\mathcal{V} > 0$ *and* $C \in \mathbb{R}$. In contrast to our findings in [12] for the original system, this demonstrates that the modified parabolic-hyperbolic system “performs significantly better” and in a far more stable manner in the asymptotically flat setting. It is interesting that the background mass $\mathcal{V}/2$ and the ADM mass m of the resulting vacuum data set are generally distinct.

5.2 Asymptotic radial expansions of vacuum initial data sets (without symmetries)

In this section we use asymptotic expansions to study the asymptotics of vacuum initial data sets obtained by the modified system Eqs. (3.8)–(3.10) for a large class of backgrounds without imposing symmetries. Assuming certain asymptotic radial expansions are valid and the free data satisfy appropriate assumptions, we demonstrate that the solutions of the constraints are *always asymptotically flat* in consistency with our findings in the spherically symmetric case in Section 5.2. In the section following this one, we then support the strong assumptions which we are required to make here by numerical computations. We focus on the modified system Eqs. (3.8)–(3.10). We refer to [12] for a corresponding result for the original system Eqs. (3.1)–(3.3) which demonstrates that general solutions of the original system are *not* asymptotically flat.

Result 2. *Let* $\Sigma = (\rho_-, \infty) \times \mathbb{S}^2$ *for some* $\rho_- > 0$. *Consider arbitrary smooth free data fields* \mathcal{R} , B_a , Q_{ab} *and* h_{ab} *on* Σ *with the properties:*

1. *The scalar function* \mathcal{R} *has an asymptotic radial expansion of order 2 such that* $\mathcal{R}^{(0)} = -1/2$ *and* $\mathcal{R}^{(1)}$ *is a strictly positive function.*
2. *The intrinsic covector field* B_a *has an asymptotic radial expansion of order 1 with* $B_a^{(0)} = 0$.
3. *The symmetric tracefree intrinsic tensor field* Q_{ab} *has an asymptotic radial expansion of order 2 with* $Q_{ab}^{(0)} = Q_{ab}^{(1)} = 0$.
4. *The symmetric intrinsic tensor field* h_{ab} *has an asymptotic radial expansion of the form* $\rho^{-2}h_{ab} = \Omega_{ab} + O(\rho^{-2})$.

Then the parabolicity and the hyperbolicity conditions, see Eqs. (3.6) and (3.13), hold for sufficiently large ρ , *and, for any solution* A , q , p_a *of the modified parabolic-hyperbolic system Eqs. (3.8)–(3.10) with the properties*

1. *A is strictly positive and has an asymptotic radial expansion of order 2,*
2. *q has an asymptotic radial expansion of order 2,*
3. *p_a is an intrinsic co-vector field with an asymptotic radial expansion of order 2,*

we find

$$q^{(0)} = q^{(1)} = 0, \quad p_a^{(0)} = p_b^{(1)} = 0, \quad A^{(0)} = 1, \quad A^{(1)} = \text{const.}$$

The vacuum initial data set corresponding to the 2 + 1-quantities $(A, q, p_a, \mathcal{R}, B_a, Q_{ab}, h_{ab})$ is therefore asymptotically flat with ADM mass $A^{(1)}$.

The conditions for the free data fields are compatible with Result 1. Observe, however, that the restriction for Q_{ab} and \mathcal{R} are in fact stronger than the ones required by Result 1. The additional condition on \mathcal{R} ensures that Eq. (3.13) holds in addition to Eq. (3.6). It is a non-trivial outcome of the analysis that Result 2 would in general not hold if $\mathcal{R}^{(0)} \neq -1/2$.

Proof of Result 2. We have discussed before

$$k^* = -\frac{2}{\rho} + O\left(\frac{1}{\rho^2}\right), \quad (5.10)$$

as a consequence of the hypothesis and that therefore Eq. (3.6) holds for sufficiently large ρ . We also find that

$$\mathcal{R} + \frac{1}{2} = \frac{\mathcal{R}^{(1)}}{\rho} + O\left(\frac{1}{\rho^2}\right) \quad (5.11)$$

and that the assumption $\mathcal{R}^{(1)} > 0$ therefore implies Eq. (3.13) for sufficiently large ρ as well. Eqs. (3.8)–(3.10) is therefore parabolic-hyperbolic asymptotically. Now we attempt to solve Eqs. (3.8)–(3.10) order by order in ρ . The two leading orders of Eq. (3.9) immediately imply $q^{(0)} = q^{(1)} = 0$. Given this, the leading order of Eq. (3.8) yields the equation

$$\hat{\Delta}A^{(0)} = -\frac{1 - (A^{(0)})^2}{A^{(0)}} =: F[A^{(0)}], \quad (5.12)$$

where $\hat{\Delta}$ is the Laplace operator associated with the round 2-sphere metric Ω_{AB} . It is clear that $A^{(0)} = 0$ cannot be a solution and we rule out all negative solutions by assumption. One positive solution is $A^{(0)} = 1$, in fact, this is the only smooth strictly positive solution: Suppose there were two different smooth strictly positive solutions $A^{(0)}$ and $\tilde{A}^{(0)}$ of Eq. (5.12). Then a standard integration by parts argument implies

$$-\|\hat{D}(A^{(0)} - \tilde{A}^{(0)})\|^2 = \left\langle A^{(0)} - \tilde{A}^{(0)}, F[A^{(0)}] - F[\tilde{A}^{(0)}] \right\rangle, \quad (5.13)$$

where the norm and the scalar product here are the standard L^2 -norm and L^2 -scalar product on the 2-sphere with respect to Ω_{ab} . One can easily check that

$$F[A^{(0)}] - F[\tilde{A}^{(0)}] = \frac{A^{(0)}\tilde{A}^{(0)} + 1}{A^{(0)}\tilde{A}^{(0)}} \left(A^{(0)} - \tilde{A}^{(0)} \right). \quad (5.14)$$

Since the fraction on the right-hand side is strictly positive if $A^{(0)}$ and $\tilde{A}^{(0)}$ are strictly positive, the right-hand side of Eq. (5.13) is therefore non-negative. Since the left-hand side

however is non-positive, this implies that $A^{(0)}$ and $\tilde{A}^{(0)}$ can differ at most by a constant. However, one can easily check that $A^{(0)} = 1$ is the only positive constant solution. Given this, the two leading orders of Eq. (3.10) imply that $p_a^{(0)} = p_a^{(1)} = 0$. Finally, we look at the third order (ρ^{-3})-term of Eq. (3.10) to get

$$\hat{\Delta}A^{(1)} = 0, \quad (5.15)$$

from which we conclude that $A^{(1)}$ is an arbitrary constant. Result 1 now implies that these solutions are asymptotically flat and that $A^{(1)}$ is the ADM mass. \square

6 Numerical investigations

6.1 Black hole background data sets

Our analytical results in Section 5 suggest that general solutions of the *modified* parabolic-hyperbolic system Eqs. (3.8)–(3.10) are asymptotically flat provided the free data satisfy certain asymptotic conditions, in contrast to solutions of the original system Eqs. (3.8)–(3.10); see [12]. In this section now we support these results by numerical calculations.

In [12] we introduced a framework to construct, in principle, multiple black hole background data sets which then provide the free data to solve the constraint equations in a next step. Here we give a short summary of our procedure which is based on the formalism presented in Section 2.2. Inspired by the ideas presented in [14] we imagine to have N black hole-like bodies at coordinate positions (x_i, y_i, z_i) with masses M_i for $i = 1, \dots, N$. Using (x, y, z) to label Cartesian coordinates on Σ and setting

$$u(x, y, z) = \sum_{i=0}^N \frac{M_i}{r_i(x, y, z)}, \quad (6.1)$$

where

$$r_i(x, y, z) = \sqrt{(x - x_i)^2 + (y - y_i)^2 + (z - z_i)^2}, \quad (6.2)$$

we define the function ρ as

$$\rho(x, y, z) = \frac{\sum_{i=0}^N M_i}{u(x, y, z)}. \quad (6.3)$$

Here we restrict to the binary case $N = 2$ and write $M_1 = M_+$, $M_2 = M_-$, $r_1 = r_+$ and $r_2 = r_-$ where

$$r_{\pm} = (0, 0, \pm Z_{\pm}), \quad (6.4)$$

for constants $Z_{\pm} \geq 0$. In contrast to [12] we now impose a “centre of mass condition” (the reason for this is given below)

$$Z_+ M_+ - Z_- M_- = 0, \quad (6.5)$$

and therefore choose

$$Z_- = Z, \quad Z_+ = \frac{M_-}{M_+} Z, \quad (6.6)$$

for some $Z \geq 0$. Notice that $M_- = 0$ together with $Z = 0$ yields the case of a *single black hole*. Fig. 1 shows examples of contour plots of the function ρ . It is clear from Fig. 1 that there is a critical value of ρ where the surfaces undergo a topology change (a *bifurcation*). For $\rho < \rho_{crit}$, each contour is the union of two disconnected 2-spheres where

$$\rho_{crit} = Z \frac{(M_+ + M_-)^2}{M_+ (\sqrt{M_+} + \sqrt{M_-})^2}. \quad (6.7)$$

However, each $\rho = \text{const}$ -surface is diffeomorphic to a *single* 2-sphere if $\rho > \rho_{crit}$. Eq. (6.7) holds under the assumption that $M_+ > 0$ and $M_-, Z \geq 0$. In all of what follows we restrict to this latter exterior regime of \mathbb{R}^3 where the collection of $\rho = \text{const}$ -surfaces give rise to a foliation. We emphasise that there certainly exist regular foliations with 2-sphere topology other than the one given by Eqs. (6.1) – (6.3) which extend arbitrarily close to the black holes in a regular fashion as well as to the asymptotic regime. Exploring the wide range of possibilities here will be important in future studies of *both* the strong field regime close to the black holes and the asymptotic far field regime. In this work here we restrict completely on the latter for which the exterior foliation given by Eqs. (6.1) – (6.3) and Eq. (6.7) is sufficient.

Finally, given all this, we pick

$$V = -2u, \quad \dot{\gamma}_{ab} = 0, \quad (6.8)$$

and

$$r = \sqrt{x^2 + y^2 + z^2}, \quad (6.9)$$

as in [12] and then obtain an initial data set (not necessarily a solution of the constraints) in the Kerr-Schild form using Section 2.2 together with Eq. (4.6). We find that the resulting data set agrees with the Schwarzschild Kerr-Schild data set with mass M_+ in the single black hole case $M_- = Z = 0$. Moreover, we see easily that Eq. (4.5) holds as a consequence of the centre of mass condition Eq. (6.5).

We can now show by direct calculations that for any M_+ , M_- and Z as above, the hypothesis of Result 2 for \mathcal{R} , B_a , Q_{ab} and h_{ab} are satisfied at least for all sufficiently large ρ . The hypothesis about the unknown fields A , q and p_a can, however, as a matter of principle, not be verified a-priori. The main purpose of the following numerical experiments is to provide evidence that the conclusions of Result 2, namely that the resulting vacuum initial data sets are always asymptotically flat, hold nevertheless.

6.2 Numerical setup

Given a background data set in Section 6.1, the next task is to numerically solve the Cauchy problem of Eqs. (3.8)–(3.10) with free data determined by this background. We

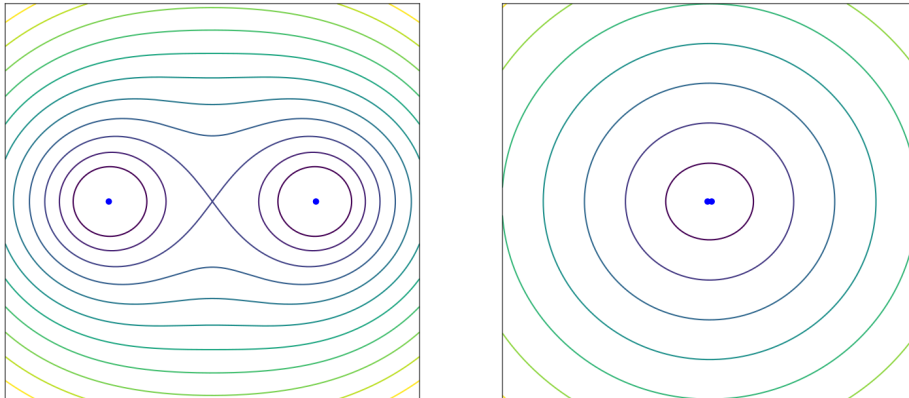


Figure 1: Contour plots of the function $\rho(x, y, z)$ defined by Eqs. (6.1) – (6.3) for $M_+ = M_- > 0$ and $Z > 0$. The left plot shows ρ close to the two black hole positions, while the right figure shows contours for large distances. Both plots restrict to the x - z -plane. It is evident that the contours become round 2-spheres in the limit of large distances.

explain below that we use two different ways to specify Cauchy data in the two following numerical examples. As discussed in more detail in [12], while the background data sets are given in Cartesian coordinates (x, y, z) on Σ , or, equivalently in corresponding spherical coordinates (r, θ, ϕ) using Eq. (6.9), the evolutions of Eqs. (3.8)–(3.10) must be performed in adapted 2+1-coordinates $(\rho, \vartheta, \varphi)$ where ρ is given by Eqs. (6.1) – (6.3) and where (ϑ, φ) are intrinsic polar coordinates on each $\rho = \text{const}$ -surface diffeomorphic to \mathbb{S}^2 . As in [12] we choose

$$\vartheta = \theta, \quad \varphi = \phi.$$

This completely fixes the coordinate transformation between the two coordinate systems (r, θ, ϕ) and $(\rho, \vartheta, \varphi)$ on Σ .

Since the exterior region is foliated by 2-spheres, we can apply the *spin-weight formalism* following [7–11, 29]. A brief summary is given in Section A in the appendix. We express the covariant derivative operator D_a (defined with respect to the intrinsic metric h_{ab}) in terms of the covariant operator \hat{D}_a defined with respect to the round unit-sphere metric Ω_{ab} ; recall that $D_a - \hat{D}_a$ can be expressed by some smooth intrinsic tensor field. Using Section A, we can then express the covariant derivative operator \hat{D}_a in terms of the \eth - and \eth' -operators [29]. Once all of this has been completed for all terms in Eqs. (3.8)–(3.10), each of these equation and each term end up with a consistent well-defined spin-weight. Most importantly, however, all terms are explicitly regular: Standard polar coordinate issues at the poles of the 2-sphere disappear when all quantities are expanded in terms of *spin-weighted spherical harmonics* and Eqs. (A.5) and (A.6) are used to calculate the intrinsic derivatives. From the numerical point of view this gives rise to a (pseudo)-spectral scheme. We can therefore largely reuse the code presented in [12] subject to two minor changes: (1) the definition of ρ now allows that $Z_+ \neq Z_-$ in agreement with Eq. (6.6), and, (2) all instances of κ in

the equations are now replaced with $\mathcal{R}q$ in agreement with our *modification* which leads to Eqs. (3.8)–(3.10). These two changes do not significantly affect our numerical methods. Once the appropriate changes were made to the code, convergence tests (analogous to the ones presented in [12]) were carried out and the appropriate behaviour was observed. All of the following simulations were carried out using the adaptive SciPy ODE solver *odeint*⁵.

Notice that the background data sets constructed in Section 6.1 are axially symmetric and hence there is no dependence on the angular coordinate $\varphi = \phi$. Motivated by this we restrict to numerical solutions of Eqs. (3.8)–(3.10) with that same symmetry in all of what follows. We can therefore restrict to the axisymmetric case of the spin-weight formalism in Section A.

6.3 Axisymmetric perturbations of single Schwarzschild black hole initial data

In this section now we use the background data set given in Section 6.1 for $M_+ = 1$ and $M_- = Z = 0$ (the “single black hole case”). The free data for Eqs. (3.8)–(3.10) are therefore given by Eq. (5.1) with $V = -1/\rho$. It follows from Section 5 that

$$\dot{q} = -\frac{2}{\rho^{3/2}\sqrt{\rho+1}}, \quad \dot{A} = \sqrt{1 + \frac{1}{\rho}}, \quad \dot{p}_a = 0, \quad (6.10)$$

is then a particular solution of Eqs. (3.8)–(3.10) representing single Schwarzschild black hole initial data of unit mass (in spherical symmetry). The point is now to generate axisymmetric (non-linear) *perturbations* of this solution by solving Eqs. (3.8)–(3.10) with the same free data, but with the following *perturbed Cauchy data* imposed at⁶ $\rho_0 = 3$:

$$q|_{\rho=\rho_0} = \dot{q}|_{\rho=\rho_0} + \varepsilon \sin(\theta), \quad A|_{\rho=\rho_0} = \dot{A}|_{\rho=\rho_0} + \varepsilon \sin(\theta), \quad p_a|_{\rho=\rho_0} = 0, \quad (6.11)$$

for some freely specifiable constant $\varepsilon \in \mathbb{R}$. For small values of ε , we can interpret the resulting vacuum initial data sets as perturbations of single Schwarzschild black hole initial data.

Given these background data and Cauchy data, we then numerically solve Eqs. (3.8)–

⁵See <https://docs.scipy.org/doc/scipy/reference/generated/scipy.integrate.odeint.html>.

⁶For the single black-hole case the foliation does not bifurcate, see Eq. (6.7), and so all values $\rho_0 > 0$ are allowed.

(3.10). Using the formalism in Section A these equations take the form

$$\partial_\rho A = -\frac{\rho}{4} \left(\frac{2}{\rho^2} (1 - 2p\bar{p}) + \left(2\mathcal{R} + \frac{1}{2} \right) q^2 \right) A^3 + \frac{1}{2\rho} (1 + A\bar{\delta}(\bar{\delta}(A))) A, \quad (6.12)$$

$$\partial_\rho q = \frac{1}{\sqrt{2}\rho^2} (\bar{\delta}(p) + \delta(\bar{p})) A - \frac{2}{\rho} \left(\frac{1}{2} - \mathcal{R} \right) q + \frac{2}{\rho^2\sqrt{2}} (p\bar{\delta}(A) + \bar{p}\delta(A)), \quad (6.13)$$

$$\partial_\rho p = A \left(\frac{1}{2} + \mathcal{R} \right) \delta(q) - \frac{2}{\rho} p + \frac{1}{\sqrt{2}} \left(\mathcal{R} - \frac{1}{2} \right) q \delta(A), \quad (6.14)$$

$$\partial_\rho \bar{p} = A \left(\frac{1}{2} + \mathcal{R} \right) \bar{\delta}(q) - \frac{2}{\rho} \bar{p} + \frac{1}{\sqrt{2}} \left(\mathcal{R} - \frac{1}{2} \right) q \bar{\delta}(A), \quad (6.15)$$

where

$$p = \frac{1}{\sqrt{2}} p_a (\partial_\vartheta^a - i \csc \theta \partial_\varphi^a), \quad \bar{p} = \frac{1}{\sqrt{2}} p_a (\partial_\vartheta^a + i \csc \theta \partial_\varphi^a), \quad (6.16)$$

and, see Eq. (5.1),

$$\mathcal{R} = -\frac{1}{2} + \frac{1}{4(1+\rho)}.$$

The quantities A and q have spin-weight zero, while p and \bar{p} have spin-weight 1 and -1 , respectively. For this particular symmetry (and the particular representation of the underlying bundle) we can assume that

$$p = \bar{p}.$$

In order to present our numerical calculations now and use them to check the predictions from Result 2 we consider the sup-norm over \mathbb{S}^2 defined, for any smooth scalar function $\mathcal{F}(\rho, \vartheta)$ (such as A and q above), as

$$\|\mathcal{F}\|(\rho) = \max_{\vartheta \in [0, \pi]} |\mathcal{F}(\rho, \vartheta)|. \quad (6.17)$$

For p_a , this norm is defined as

$$\|p\|(\rho) = \max_{\vartheta \in [0, \pi]} \sqrt{\Omega^{ab} p_a(\rho, \vartheta) p_b(\rho, \vartheta)} = \max_{\vartheta \in [0, \pi]} \sqrt{p(\rho, \vartheta) \bar{p}(\rho, \vartheta)}. \quad (6.18)$$

In a first instance, we expect the following behaviour

$$\|A - 1\|(\rho) = O\left(\frac{1}{\rho}\right), \quad \|q\|(\rho) = O\left(\frac{1}{\rho^2}\right), \quad \|p\|(\rho) = O\left(\frac{1}{\rho^2}\right) \quad (6.19)$$

for all of the solutions above according to Result 2. Fig. 2 shows that the numerical solutions are indeed consistent with this. The particular numerical solution shown there was produced with $\varepsilon = 10^{-2}$, an absolute and relative error tolerance for the adaptive ODE solver of 10^{-12} , and for $N = 11$, where N is the number of spatial points in the ϑ -direction. We have repeated the same numerical experiments with smaller values of ε as well and found the same qualitative behaviour in agreement with Result 2.

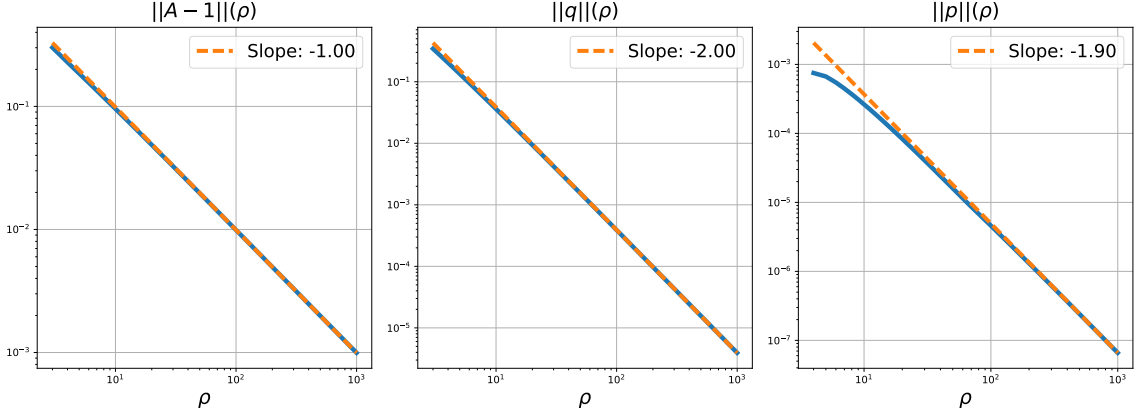


Figure 2: Decay plots of the numerical solution for the “single black hole case” obtained with $\epsilon = 10^{-2}$, $N = 11$ and a numerical error tolerance of 10^{-12} .

However, in order to be demonstrate full consistency with Result 2 we must show that

$$A = 1 + \frac{A^{(1)}}{\rho} + O\left(\frac{1}{\rho^2}\right), \quad (6.20)$$

for a *constant* $A^{(1)}$ (which then represents the ADM mass). We proceed as follows to numerically support the claim that this is indeed true. If the first two orders of A are constant with respect to ϑ , then the quantity, see Eqs. (A.9) and (A.10),

$$1 - \frac{4\pi|\underline{A}(\rho)|^2}{\|A(\rho)\|_{L^2(\mathbb{S}^2)}} = \frac{\|A(\rho)\|_{L^2(\mathbb{S}^2)} - 4\pi|\underline{A}(\rho)|^2}{\|A(\rho)\|_{L^2(\mathbb{S}^2)}} = \frac{\sum_{\ell=1}^{\infty} |A_{\ell}(\rho)|^2}{\sum_{\ell=0}^{\infty} |A_{\ell}(\rho)|^2} \quad (6.21)$$

must decay like $O(\rho^{-4})$. In Fig. 3 we see that this is indeed the case for $\epsilon = 10^{-2}$.

Let us now discuss how we numerically calculate the ADM mass. In accordance with Result 2, we have

$$\underline{A}(\rho) = 1 + \frac{A^{(1)}}{\rho} + O\left(\frac{1}{\rho^2}\right), \quad (6.22)$$

see Eq. (A.8). Since $\underline{A}^{(1)} = A^{(1)}$ follows from the above, we therefore find

$$A^{(1)} = \rho(\underline{A}(\rho) - 1) + O\left(\frac{1}{\rho}\right). \quad (6.23)$$

This suggests that we define

$$m_N(\rho) = \rho(\underline{A}(\rho) - 1), \quad (6.24)$$

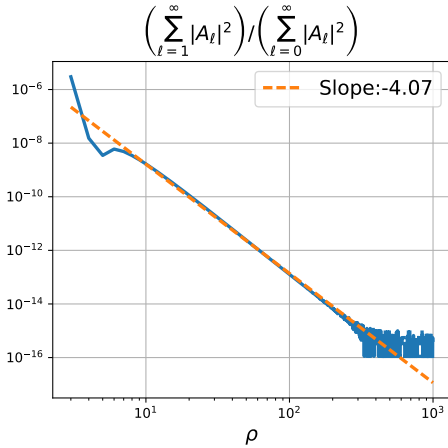


Figure 3: Mode decay plot of the numerical solution for the “single black hole case” obtained with the same parameters as Fig. 2.

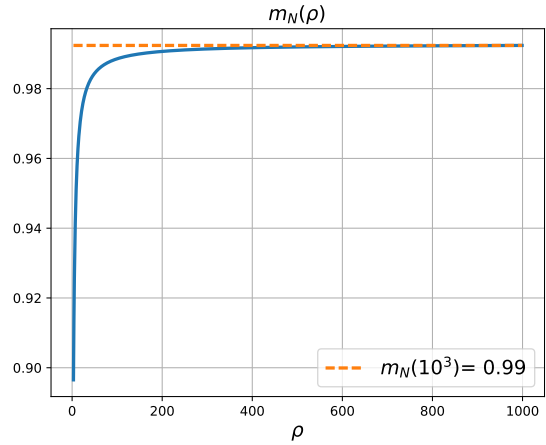


Figure 4: Estimate the ADM mass for the “single black hole case” obtained with the same parameters as Fig. 2.

as a numerical estimate for the ADM mass m_{ADM} . In particular, we get

$$m_N(\rho) = m_{ADM} + O\left(\frac{1}{\rho}\right), \quad (6.25)$$

as confirmed by Fig. 4. Given all this it becomes clear that the numerical estimate for the mass m_N becomes better as ρ becomes larger. We find, however, that the numerical errors in numerically solving the constraints become significant if we go further than $\rho \sim 10^3$. It is natural then to wonder how good the approximation $m_{ADM} = m_N(10^3)$ is. For this we consider the quantity

$$\mathcal{E}_A[m_{ADM}] = |m_N(2\rho) - m_N(\rho)|, \quad (6.26)$$

which is calculated for $\rho = 10^3$ as a measure of the absolute error. For our example case, with $\epsilon = 10^{-2}$, we find

$$m_{ADM} = 0.9942, \quad \mathcal{E}_A[m_{ADM}] = 2.34 \times 10^{-6}. \quad (6.27)$$

Notice that the relative error is of order $\sim 10^{-6}$. As was mentioned above, this is likely due to the error associated with measuring m_{ADM} at a *finite* value of ρ . However, due to the errors generated by numerically solving the constraints for very large values of ρ , we need to accept whatever error we have at that point in the measurement of the mass.

6.4 Binary black hole-like initial data sets

In this subsection we repeat essentially the same numerical experiments as before with two changes: (1), the background data set is now determined with parameters $M_+ = M_- = 1/2$

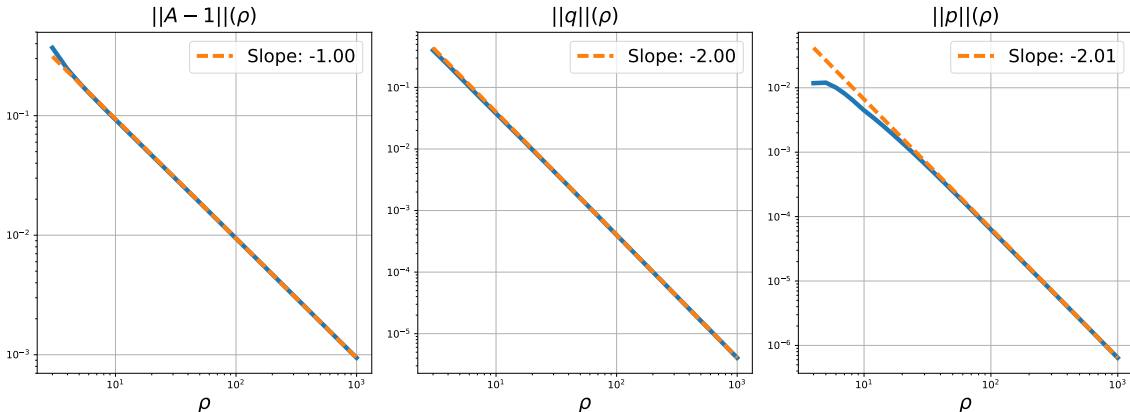


Figure 5: Decay plots of the numerical solution for the “binary black hole case” obtained with $M_+ = M_- = 1/2$, $Z = 1$, $N = 11$, $\rho_0 = 3$ and a numerical error tolerance of 10^{-12} .

and $Z = 1$ (an “equal mass binary black hole case”), and (2), instead of the “perturbed” Cauchy data as in Eq. (6.11), we now choose the values obtained from the background data set at $\rho_0 = 3$. For this particular case Eq. (6.7) gives that the bifurcation occurs at $\rho_{crit} = 1$.

Our numerical findings, as shown in Fig. 5, are again consistent with the prediction

$$\|A - 1\|(\rho) = O\left(\frac{1}{\rho}\right), \quad \|q\|(\rho) = O\left(\frac{1}{\rho^2}\right), \quad \|p\|(\rho) = O\left(\frac{1}{\rho^2}\right) \quad (6.28)$$

from Result 2. Similarly, as with the single black hole case, we expect the quantity

$$\frac{\sum_{\ell=1}^{\infty} |A_{\ell}(\rho)|^2}{\sum_{\ell=0}^{\infty} |A_{\ell}(\rho)|^2} \quad (6.29)$$

to decay like $O(\rho^{-4})$. In Fig. 6 we observe exactly this behaviour. As before, we interpret this as strong evidence that the obtained vacuum initial data sets are indeed asymptotically flat. One may therefore use Eq. (6.24) to numerically estimate the ADM mass; the behaviour predicted by Eq. (6.25) is verified in Fig. 7. We find

$$m_{ADM} = 0.9423, \quad \mathcal{E}_A[m_{ADM}] = 5.01 \times 10^{-6}. \quad (6.30)$$

We have repeated the calculations for similar parameter sets and came to the same conclusions: The resulting vacuum initial data sets are always asymptotically flat. Given fixed values of M_+ and M_- , say, $M_+ = M_- = 1/2$ as before, one expects the resulting ADM masses to depend strongly on the separation distance Z . To investigate this we numerically calculate the resulting vacuum initial data sets and ADM masses for a range of separation distances Z . Note that since we treat $\rho_0 = 3$ as fixed, Eq. (6.7) introduces an upper bound for the possible values for Z , namely $Z < \rho_{crit}$. The results are shown in Fig. 8, where we see that the ADM mass is a decreasing function of the separation distance Z . Notice that the same dependence of the ADM-mass on Z had been observed in [12] for asymptotically Euclidean data sets.

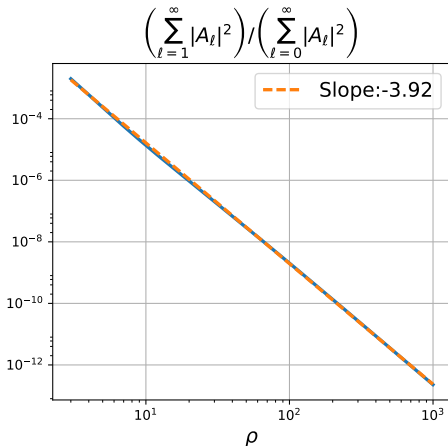


Figure 6: Mode decay plot of the numerical solution for the “binary black hole case” obtained with the same parameters as Fig. 5.

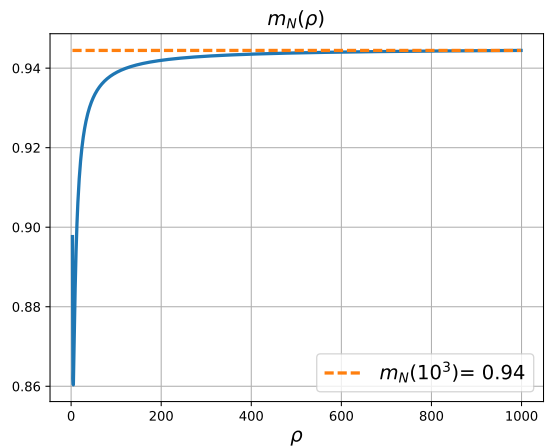


Figure 7: Estimate of the ADM mass for the “binary black hole case” obtained with the same parameters as Fig. 5.

7 Conclusions

In this paper we propose a new parabolic-hyperbolic formulation of the Einstein vacuum constraints based on a formulation originally given by Rácz. Using analytical and numerical methods we provide strong evidence that the main major drawback of these kinds of evolutionary formulations, namely to generically produce vacuum initial data sets which violate asymptotically flatness [10, 12, 19], has now finally been overcome.

In Sections 6.3 and 6.4 we have numerically constructed particular vacuum initial data sets as solutions of our new equations which could potentially be interpreted as perturbed Schwarzschild initial data and as binary black hole initial data, respectively. As we discussed, the particular choice of foliation (see Section 6.1) leads to the restriction $\rho > \rho_{crit}$ with Eq. (6.7). This means that we only have limited access to the strong field regime close to the black holes. Strictly speaking it is therefore not even clear whether the resulting vacuum initial data sets really represent black holes. In order to resolve this issue, we need to find for example apparent horizons in the strong field regime. Given that the asymptotics of the resulting initial data sets are under control now, future studies will therefore have to focus on a remedy for the issues associated with the strong field regime. A natural starting point for such studies would be to try to come up with a different 2-sphere foliation than the one in Section 6.1, which matches the one above for sufficiently large values of ρ , but which allows to place the *initial 2-surface arbitrarily close to the black holes*. All this would need to be done in a way which guarantees that k^* is strictly negative, which might be a non-trivial condition given how involved and non-trivial typical strong field geometries can be. In any case, if this can be achieved, then we can use Eqs. (3.8)–(3.10) to construct

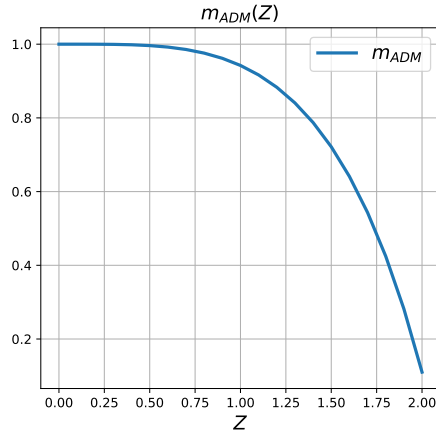


Figure 8: Dependence of m_{ADM} on Z in the “binary black hole case” with $M_+ = M_- = 1/2$, $\rho_0 = 3$, $N = 11$ and numerical error tolerance of 10^{-12} .

asymptotically flat vacuum initial data sets and analyse in great detail the resulting strong field black hole-like regimes.

Acknowledgements

JR is supported by a Ph.D scholarship awarded by the University of Otago. Part of this research was funded by a grant to JF from the Division of Sciences of the University of Otago.

Appendices

A Spin-weight and spin-weighted spherical harmonics

We say that a function f defined on \mathbb{S}^2 has *spin-weight* s if it transforms as $f \rightarrow e^{is\xi} f$ under a local rotation by an angle ξ in the tangent plane at any point in \mathbb{S}^2 . Let (ϑ, φ) be standard polar coordinates on \mathbb{S}^2 . If f has spin-weight s and is sufficiently smooth, it can be written as

$$f(\vartheta, \varphi) = \sum_{l=|s|}^{\infty} \sum_{m=-l}^l f_{lm} s Y_{lm}(\vartheta, \varphi), \quad (\text{A.1})$$

where ${}_s Y_{lm}(\vartheta, \varphi)$ are the *spin-weighted spherical harmonics (SWSH)* and where f_{lm} are complex numbers. Using the conventions in [7–11, 29], these functions satisfy

$$\int_{\mathbb{S}^2} {}_s Y_{l_1 m_1}(\vartheta, \varphi) {}_s \bar{Y}_{l_2 m_2}(\vartheta, \varphi) d\Omega = \delta_{l_1 l_2} \delta_{m_1 m_2}, \quad (\text{A.2})$$

where δ_{lm} is the Kronecker delta and $d\Omega$ is the area element of the metric of the round unit sphere. Using this we find that the coefficients f_{lm} in Eq. (A.1) can be calculated as

$$f_{lm} = \int_{\mathbb{S}^2} f(\vartheta, \varphi) {}_s \bar{Y}_{lm}(\vartheta, \varphi) d\Omega. \quad (\text{A.3})$$

The *eth-operators* $\bar{\partial}$ and $\bar{\partial}'$ are defined by

$$\bar{\partial} f = \partial_\vartheta f - \frac{i}{\sin \vartheta} \partial_\varphi f - s f \cot \vartheta, \quad \bar{\partial}' f = \partial_\vartheta f + \frac{i}{\sin \vartheta} \partial_\varphi f + s f \cot \vartheta, \quad (\text{A.4})$$

for any function f on \mathbb{S}^2 with spin-weight s . We have

$$\bar{\partial} {}_s Y_{lm}(\vartheta, \varphi) = -\sqrt{(l-s)(l+s+1)} {}_{s+1} Y_{lm}(\vartheta, \varphi), \quad (\text{A.5})$$

$$\bar{\partial}' {}_s Y_{lm}(\vartheta, \varphi) = \sqrt{(l+s)(l-s+1)} {}_{s-1} Y_{lm}(\vartheta, \varphi), \quad (\text{A.6})$$

$$\bar{\partial}' \bar{\partial} {}_s Y_{lm}(\vartheta, \varphi) = -(l-s)(l+s+1) {}_s Y_{lm}(\vartheta, \varphi). \quad (\text{A.7})$$

Thus, using the properties above it is easy to see that $\bar{\partial}$ raises the spin-weight by one while $\bar{\partial}'$ lowers it by one.

The *average* of a function f with spin-weight 0 on \mathbb{S}^2 is defined by

$$\underline{f} = \frac{1}{4\pi} \int_{\mathbb{S}^2} f d\Omega. \quad (\text{A.8})$$

Expressing f in terms of SWSH and using Eq. (A.2) it follows

$$\begin{aligned} \underline{f} &= \frac{1}{4\pi} \int_{\mathbb{S}^2} \sum_{l=0}^{\infty} \sum_{m=-l}^l f_{lm} {}_0 Y_{lm}(\vartheta, \varphi) d\Omega, \\ &= \frac{\sqrt{4\pi}}{4\pi} \int_{\mathbb{S}^2} \sum_{l=0}^{\infty} \sum_{m=-l}^l f_{lm} {}_0 Y_{lm}(\vartheta, \varphi) {}_0 \bar{Y}_{00}(\vartheta, \varphi) d\Omega, \\ &= \frac{1}{\sqrt{4\pi}} f_{00}, \end{aligned} \quad (\text{A.9})$$

where we have used the fact that ${}_0 Y_{00}(\vartheta, \varphi) = (4\pi)^{-1/2}$. Another quantity of interest is the L^2 -norm with respect to the standard round metric on S^2 . The *Parseval identity* states that

$$\|f\|_{L^2(\mathbb{S}^2)}^2 = \sum_{l=0}^{\infty} \sum_{m=-l}^l |f_{lm}|^2. \quad (\text{A.10})$$

Finally we notice that many quantities considered in this paper are axially symmetric and therefore do not depend on the angle φ . For such functions, all coefficients with f_{lm} with $m \neq 0$ vanish and we use the following short-hand notation to write Eq. (A.1) as

$$f(\vartheta) = \sum_{l=|s|}^{\infty} f_{l s} Y_l(\vartheta). \quad (\text{A.11})$$

References

- [1] M. Alcubierre. *Introduction to 3+1 Numerical Relativity*. Oxford Science Publications, 2008.
- [2] M. T. Anderson. On the conformal method for the Einstein constraint equations. 2018. Preprint. [arXiv:1812.06320](https://arxiv.org/abs/1812.06320).
- [3] R. A. Bartnik. Quasi-spherical metrics and prescribed scalar curvature. *J. Diff. Geom.*, 37(1):31–71, 1993. DOI: [10.4310/jdg/1214453422](https://doi.org/10.4310/jdg/1214453422).
- [4] R. A. Bartnik and J. Isenberg. The Constraint Equations. In *The Einstein Equations and the Large Scale Behavior of Gravitational Fields*, pages 1–38. Birkhäuser, Basel, 2004.
- [5] T. W. Baumgarte and S. L. Shapiro. *Numerical Relativity. Solving Einstein’s Equations on the Computer*. Cambridge University Press, 2010.
- [6] F. Beyer. A spectral solver for evolution problems with spatial S^3 -topology. *J. Comp. Phys.*, 228(17):6496–6513, 2009. DOI: [10.1016/j.jcp.2009.05.037](https://doi.org/10.1016/j.jcp.2009.05.037).
- [7] F. Beyer, B. Daszuta, and J. Frauendiener. A spectral method for half-integer spin fields based on spin-weighted spherical harmonics. *Class. Quantum Grav.*, 32(17):175013, 2015. DOI: [10.1088/0264-9381/32/17/175013](https://doi.org/10.1088/0264-9381/32/17/175013).
- [8] F. Beyer, B. Daszuta, J. Frauendiener, and B. Whale. Numerical evolutions of fields on the 2-sphere using a spectral method based on spin-weighted spherical harmonics. *Class. Quantum Grav.*, 31(7):075019, 2014. DOI: [10.1088/0264-9381/31/7/075019](https://doi.org/10.1088/0264-9381/31/7/075019).
- [9] F. Beyer, L. Escobar, and J. Frauendiener. Numerical solutions of Einstein’s equations for cosmological spacetimes with spatial topology S^3 and symmetry group $U(1)$. *Phys. Rev. D*, 93(4):043009, 2016. DOI: [10.1103/PhysRevD.93.043009](https://doi.org/10.1103/PhysRevD.93.043009).
- [10] F. Beyer, L. Escobar, and J. Frauendiener. Asymptotics of solutions of a hyperbolic formulation of the constraint equations. *Class. Quantum Grav.*, 34(20):205014, 2017. DOI: [10.1088/1361-6382/aa8be6](https://doi.org/10.1088/1361-6382/aa8be6).

- [11] F. Beyer, L. Escobar, and J. Frauendiener. Criticality of inhomogeneous Nariai-like cosmological models. *Phys. Rev. D*, 95(8):084030, 2017. DOI: [10.1103/PhysRevD.95.084030](https://doi.org/10.1103/PhysRevD.95.084030).
- [12] F. Beyer, L. Escobar, J. Frauendiener, and J. Ritchie. Numerical construction of initial data sets of binary black hole type using a parabolic-hyperbolic formulation of the vacuum constraint equations. *Class. Quantum Grav.*, 36(17):175005, 2019. DOI: [10.1088/1361-6382/ab3482](https://doi.org/10.1088/1361-6382/ab3482).
- [13] N. T. Bishop, F. Beyer, and M. Koppitz. Black hole initial data from a nonconformal decomposition. *Phys. Rev. D*, 69(6):064010, 2004. DOI: [10.1103/PhysRevD.69.064010](https://doi.org/10.1103/PhysRevD.69.064010).
- [14] N. T. Bishop, R. Isaacson, M. Maharaj, and J. Winicour. Black hole data via a Kerr-Schild approach. *Phys. Rev. D*, 57(10):6113–6118, 1998. DOI: [10.1103/PhysRevD.57.6113](https://doi.org/10.1103/PhysRevD.57.6113).
- [15] C. Cederbaum, J. Cortier, and A. Sakovich. On the Center of Mass of Asymptotically Hyperbolic Initial Data Sets. *Ann. Henri Poincaré*, 17(6):1505–1528, 2016. DOI: [10.1007/s00023-015-0438-5](https://doi.org/10.1007/s00023-015-0438-5).
- [16] Y. Choquet-Bruhat and R. P. Geroch. Global aspects of the Cauchy problem in general relativity. *Commun. Math. Phys.*, 14(4):329–335, 1969. DOI: [10.1007/BF01645389](https://doi.org/10.1007/BF01645389).
- [17] Y. Choquet-Bruhat, J. Isenberg, and J. W. York. Einstein constraints on asymptotically Euclidean manifolds. *Phys. Rev. D*, 61(8), 2000. DOI: [10.1103/PhysRevD.61.084034](https://doi.org/10.1103/PhysRevD.61.084034).
- [18] T. Chu. Including realistic tidal deformations in binary black-hole initial data. *Phys. Rev. D*, 89(6):064062, 2014. DOI: [10.1103/PhysRevD.89.064062](https://doi.org/10.1103/PhysRevD.89.064062).
- [19] K. Csukás and I. Rácz. On the asymptotics of solutions to the evolutionary form of the constraints. 2019. Preprint. [arXiv:1911.02900](https://arxiv.org/abs/1911.02900).
- [20] S. Dain and H. Friedrich. Asymptotically Flat Initial Data with Prescribed Regularity at Infinity. *Commun. Math. Phys.*, 222(3):569–609, 2001. DOI: [10.1007/s002200100524](https://doi.org/10.1007/s002200100524).
- [21] J. Dilts, M. Holst, T. Kozareva, and D. Maxwell. Numerical Bifurcation Analysis of the Conformal Method. 2017. Preprint. [arXiv:1710.03201](https://arxiv.org/abs/1710.03201).
- [22] G. Doulis. Construction of high precision numerical single and binary black hole initial data. *Phys. Rev. D*, 100(2):024064, 2019. DOI: [10.1103/PhysRevD.100.024064](https://doi.org/10.1103/PhysRevD.100.024064).
- [23] Y. Fourès-Bruhat. Théorème d’existence pour certains systèmes d’équations aux dérivées partielles non linéaires. *Acta Math.*, 88(1):141–225, 1952. DOI: [10.1007/BF02392131](https://doi.org/10.1007/BF02392131).
- [24] S. W. Hawking. Gravitational Radiation in an Expanding Universe. *J. Math. Phys.*, 9(4):598–604, 1968. DOI: [10.1063/1.1664615](https://doi.org/10.1063/1.1664615).

- [25] G. Lovelace. Reducing spurious gravitational radiation in binary-black-hole simulations by using conformally curved initial data. *Class. Quantum Grav.*, 26(11):114002, 2009. DOI: [10.1088/0264-9381/26/11/114002](https://doi.org/10.1088/0264-9381/26/11/114002).
- [26] R. A. Matzner, M. F. Huq, and D. Shoemaker. Initial data and coordinates for multiple black hole systems. *Phys. Rev. D*, 59(2):024015, 1998. DOI: [10.1103/PhysRevD.59.024015](https://doi.org/10.1103/PhysRevD.59.024015).
- [27] C. Moreno, D. Núñez, and O. Sarbach. Kerr–Schild-type initial data for black holes with angular momenta. *Class. Quantum Grav.*, 19(23):6059–6073, 2002. DOI: [10.1088/0264-9381/19/23/312](https://doi.org/10.1088/0264-9381/19/23/312).
- [28] A. Nakonieczna, L. Nakonieczny, and I. Rącz. Black hole initial data by numerical integration of the parabolic-hyperbolic form of the constraints. 2017. Preprint. [arXiv:1712.00607](https://arxiv.org/abs/1712.00607).
- [29] R. Penrose and W. Rindler. *Two-Spinor Calculus and Relativistic Fields*, volume 1 of *Spinors and Space-Time*. Cambridge University Press, Cambridge, 1984.
- [30] I. Rącz. Is the Bianchi identity always hyperbolic? *Class. Quantum Grav.*, 31(15):155004, 2014. DOI: [10.1088/0264-9381/31/15/155004](https://doi.org/10.1088/0264-9381/31/15/155004).
- [31] I. Rącz. Cauchy problem as a two-surface based ‘geometrodynamics’. *Class. Quantum Grav.*, 32(1):015006, 2015. DOI: [10.1088/0264-9381/32/1/015006](https://doi.org/10.1088/0264-9381/32/1/015006).
- [32] I. Rącz. Constraints as evolutionary systems. *Class. Quantum Grav.*, 33(1):015014, 2016. DOI: [10.1088/0264-9381/33/1/015014](https://doi.org/10.1088/0264-9381/33/1/015014).
- [33] I. Rącz. On the Evolutionary Form of the Constraints in Electrodynamics. *Symmetry*, 11(1):10, 2018. DOI: [10.3390/sym11010010](https://doi.org/10.3390/sym11010010).
- [34] I. Rącz and J. Winicour. Black hole initial data without elliptic equations. *Phys. Rev. D*, 91(12):124013, 2015. DOI: [10.1103/PhysRevD.91.124013](https://doi.org/10.1103/PhysRevD.91.124013).
- [35] I. Rącz and J. Winicour. Toward computing gravitational initial data without elliptic solvers. *Class. Quantum Grav.*, 35(13):135002, 2018. DOI: [10.1088/1361-6382/aac5c5](https://doi.org/10.1088/1361-6382/aac5c5).
- [36] L. B. Szabados. Quasi-Local Energy-Momentum and Angular Momentum in General Relativity. *Living Rev. Relativity*, 12(4):4, 2009. DOI: [10.12942/lrr-2009-4](https://doi.org/10.12942/lrr-2009-4).
- [37] J. Winicour. The algebraic-hyperbolic approach to the linearized gravitational constraints on a Minkowski background. *Class. Quantum Grav.*, 34(15):157001, 2017. DOI: [10.1088/1361-6382/aa7bd6](https://doi.org/10.1088/1361-6382/aa7bd6).